ORIGINAL SCIENTIFIC PAPER

CROATICA CHEMICA ACTA

Croat. Chem. Acta **2025**, *98*(1), 15–26
Published online: March 20, 2025
DOI: 10.5562/cca4137

HKD 1926

FOX-Inspired Optimizer with Support Vector Regression Modeling of Water-Based $CaCO_3$-CuO-SiO_2 Trihybrid Nanofluids Thermal Properties: Comparative Study

Amel Euldji,[1] Maamar Laidi,[1] Mohamed Hentabli,[1,2,3,*] Achouak Madani,[1] Salah Hanini[1]

[1] Laboratory of Biomaterials and Transfer Phenomena, Theoretical and Computational Chemistry in Process Engineering Team, University Yahia Fares of Médéa, Algeria
[2] Process Engineering Department, Faculty of Technology, University of Chlef, P.O Box. 151, Hay Essalem, Chlef, 02000, Algeria
[3] Laboratory of Vegetal Chemistry-Water-Energy,University of Hassiba BenBouali, B.P. 151, Chlef 02000, Algeria
* Corresponding author's e-mail address: hentabli.mohamed92@gmail.com & hentabli.mohamed@univ-medea.dz

RECEIVED: October 22, 2024 ✶ REVISED: January 23, 2025 ✶ ACCEPTED: January 23, 2025

Abstract: Recent advances in artificial intelligence have spurred significant interest in accurately predicting the thermophysical properties and rheological behavior of nanofluids. This study introduces four support vector regression (SVR) models optimized using the Dragonfly Algorithm (DA) and the novel FOX-inspired Optimization Algorithm (FOA). The models were evaluated with two cross-validation techniques, Leave-M-Out (LMO) and Holdout, to estimate the thermal properties of trihybrid nanofluids (THNFs). Trained and tested on a diverse dataset compiled from published experimental studies, these models exhibited exceptional predictive accuracy. Performance evaluation using metrics such as mean squared error (*MSE*) and Theil's U^2 revealed remarkably low error values, with all models achieving correlation coefficients (R) and determination coefficients (R^2) exceeding 0.999. The results demonstrate the superior capability of these models to predict dynamic viscosity and thermal conductivity with high precision. This study's findings hold substantial industrial significance, particularly in energy, thermal management, and manufacturing sectors.

Keywords: FOX-inspired optimization algorithm, Rheology, Support vector machine, Dragonfly algorithm, Trihybrid Nanofluid, Thermophysical Properties.

INTRODUCTION

HYBRID nanofluids, synthesized by suspending two or more types of nanoparticles in base fluids, represent an evolution of conventional nanofluids. These advanced fluids demonstrate superior heat transfer properties, including higher heat transfer coefficients and Nusselt numbers, compared to mono nanofluids.[1] Such improvements make hybrid nanofluids a promising solution for applications in heat pipes, heat exchangers, automotive systems, nuclear cooling, biomedical fields, and more.[2,3]
The effectiveness of hybrid nanofluids in convective heat transfer depends critically on their thermophysical properties, including: density, specific heat and predominantly on the thermal conductivity and viscosity as they are the most influential parameters. Research has shown that nanoparticles with high thermal conductivity enhance the thermal conductivity of the base fluid, leading to improved convective heat transfer;[4] for example, studies on Cu-water nanofluids[5] and Al_2O_3-water nanofluids[6] have confirmed that increasing nanoparticle concentrations result in significant enhancements in thermal conductivity and, consequently, the heat transfer coefficient.

The addition of nanoparticles also alters other thermophysical properties, such as viscosity, which can either enhance or hinder performance. For instance, Ehsan et al.[6] demonstrated that increasing the volume fraction of multi-walled carbon nanotubes (MWCNTs) in a water-ethylene glycol base improved the heat transfer coefficient

by 44 % at specific temperatures and concentrations, despite increased viscosity.[7] This synergistic interplay between nanoparticles underscores the importance of optimizing particle combinations for maximum efficiency.

While hybrid nanofluids generally outperform mono-nanofluids due to their synergistic effects, achieving optimal thermophysical properties depends on factors such as nanoparticle type, mixing ratios, and operating conditions. Studies on binary hybrid nanofluids have demonstrated significant improvements in thermal conductivity and viscosity under specific mixing ratios;[8] however, the complexity of ternary (trihybrid) nanofluids introduces additional challenges, such as identifying the optimal nanoparticle combination and mixing ratio.

Empirical correlations, regression models, and machine-learning techniques were employed to predict the thermophysical properties of hybrid nanofluids. For instance, researchers have developed regression models with high accuracy for binary hybrid nanofluids,[9] but these models often fail to generalize across varying mixed ratios or complex systems like trihybrid nanofluids. Machine-learning methods, including: Artificial Neural Networks (ANN), Boosted Regression Tree (BRT) and Support Vector Machine (SVM), have promising outcome in addressing these limitations;[10–14] nonetheless, most existing studies focus on binary nanofluids, leaving a significant gap in understanding and predicting the properties of trihybrid nanofluids.

This study aims to address this gap by applying advanced machine-learning techniques based on Support Vector Regression (SVR) optimized with the Dragonfly Algorithm (DA) and the FOX-inspired Optimization Algorithm (FOA) to model the thermophysical properties of trihybrid nanofluids. By leveraging experimental data, this work seeks to predict the nonlinear relationships between thermal conductivity, viscosity and their governing factors; hence, providing a robust framework for optimizing nanofluid formulations. This research not only enhances the understanding of trihybrid nanofluids but also sets a foundation for their practical application in advanced thermal systems.

METHODOLOGY

Data Description

Data used in this study, amassed from previously published experimental studies, is summarized in Table 1.

To identify outliers or errors in the dataset, the statistical description is showcased in Table 2. This table provides a comprehensive statistical analysis of the dataset used in this research. The data exhibit variations across the measured properties; for instance, the average content of VR_1 ranged from 0.25 % to 0.60 %, with a standard deviation of 0.15 %. Interestingly, the distribution of VR_1 content leans slightly towards higher values, as indicated by a positive skewness (0.0384). Similar trends are observed for other features, with standard deviations highlighting the data's variability. These insights into the data's central tendency, dispersion, and skewness will be crucial for effectively applying the SVR models and interpreting the obtained results.[15]

Violin plots are useful for visualizing the distribution of data and comparing distributions between different groups or categories within a dataset. The horizontal line in each box represents the median value, and the box encompasses the interquartile range (IQR) containing half of the data. The whiskers extend to the minimum and maximum values, excluding outliers.

Multicollinearity Analysis

Multicollinearity analysis is a statistical technique used to assess the linear relationship between two or more independent variables in a regression model. High multicollinearity can cause problems in regression analysis, leading to inflated standard errors and making it difficult to interpret the coefficients of individual variables.

An assessment of multicollinearity was conducted by examining the correlation matrix. This analysis revealed

Table 1. Experimental studies previously published of various aqueous trihybrid nanofluids together with SDS as a surfactant for different volume ratios.

Nanoparticles/base fluid	Solid volume concentration range / %	T / °C	nanofluid type (VR: volume ratios)	Data points	Ref.
CuO-$CaCO_3$-SiO_2 / DW	0.1–0.5	15–60	A (0.33, 0.33, 0.33) B (0.50, 0.25, 0.25) C (0.60, 0.30, 0.10) D (0.25, 0.50, 0.25) E (0.25, 0.25, 0.50)	360	[14]

Table 2. Statistical analysis data.

Variables	$VR_1 = CuO$	$VR_2 = CaCO_3$	$VR_3 = SiO_2$	VF / %	T /°C	μ / mPa s^{-1}	λ_{thnf} / W m^{-1} K^{-1}
Min	0.2500	0.2500	0.1000	0.0000	14.5893	0.4543	0.5764
Max	0.6000	0.5000	0.5000	0.5000	60.2995	1.7074	0.9495
Range	0.3500	0.2500	0.4000	0.5000	45.7102	1.2531	0.3731
Mean	0.4222	0.3222	0.2556	0.2500	37.4625	0.8797	0.7504
Geomean mean	0.3942	0.3128	0.2169	0.0000	34.3863	0.8383	0.7457
Harmmean mean	0.3673	0.3051	0.1818	0.0000	31.1419	0.8000	0.7408
Trimmean	0.4219	0.3164	0.2506	0.2500	37.4578	0.8653	0.7497
Kurtosis	1.2421	3.3966	2.1962	1.7314	1.7796	2.7378	2.4875
Moment	0.0001	0.0008	0.0013	0.0000	4.1921	0.0146	0.0000
Skewness	0.0384	1.3242	0.4788	0.0000	0.0014	0.6798	0.0234
Median Absolute Deviation	0.1445	0.0630	0.1074	0.1500	12.4916	0.2298	0.0680
Standard Deviation	0.1510	0.0849	0.1382	0.1710	14.3808	0.2784	0.0845
Interquartile range	0.3500	0.0833	0.2333	0.3000	24.9907	0.4199	0.1083
Variance	0.0228	0.0072	0.0191	0.0292	206.8068	0.0775	0.0071

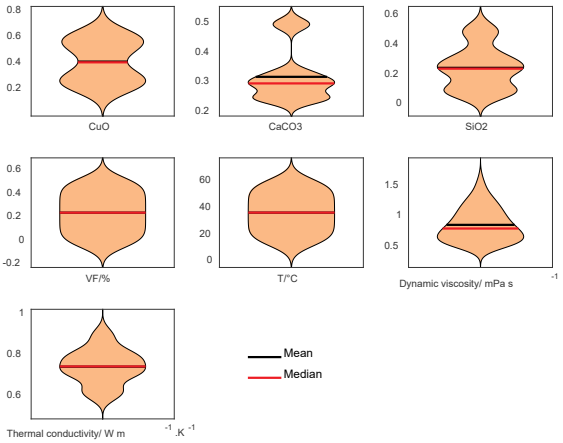

Figure 1. Violin plots illustrating the distribution of the experimental dataset used in this study. The dataset includes, for the three nanoparticles CuO, $CaCO_3$ and SiO_2, the following: the volume ratios (VF), the volume fraction, the temperature (T / °C), the dynamic viscosity (in mPa·s^{-1}) and the thermal conductivity (in W·m^{-1}·K^{-1}). Each violin plot shows the spread of values and the density of data points for each parameter, providing insight into the variability within the dataset. The volume fraction represents the proportion of nanoparticles in the hybrid nanofluids, while the temperature indicates the testing conditions. The dynamic viscosity and thermal conductivity are the two target properties predicted by the models.

minimal linear relationships between the independent variables. The absence of strong correlations between these variables suggests a low risk of multicollinearity in the regression model. This is a positive finding, as multicollinearity can lead to inflated standard errors and hinder the interpretability of individual variable coefficients.

Integration of Metaheuristic Algorithms with Support Vector Regression for Predicting Thermophysical Properties

Support Vector Regression (SVR) is a robust machine learning algorithm derived from Support Vector Machines (SVM), initially introduced by Vapnik et al. in 1995.[16] SVR is specifically designed to address regression tasks by finding an optimal function that predicts continuous values with minimal error.[17] Unlike traditional regression models, SVR focuses on identifying a hyperplane that maximizes the margin of tolerance around the predicted values, known as the ε-insensitive zone. This characteristic makes SVR particularly suitable for handling nonlinear relationships between input features and target variables, a frequent challenge in predicting thermophysical properties of nanofluids.[18]

The accuracy and generalization capacity of an SVR model are highly dependent on selecting suitable hyperparameters, including the penalty parameter (C), the kernel parameter (σ), and the insensitive parameter (ε).[13,19] These hyperparameters govern the trade-off between model complexity and prediction error, the ability to capture nonlinear patterns and the tolerance to small deviations from the observed data, respectively; additionally, determining the optimal combination of these parameters is a non-trivial task, as it involves navigating a high-dimensional

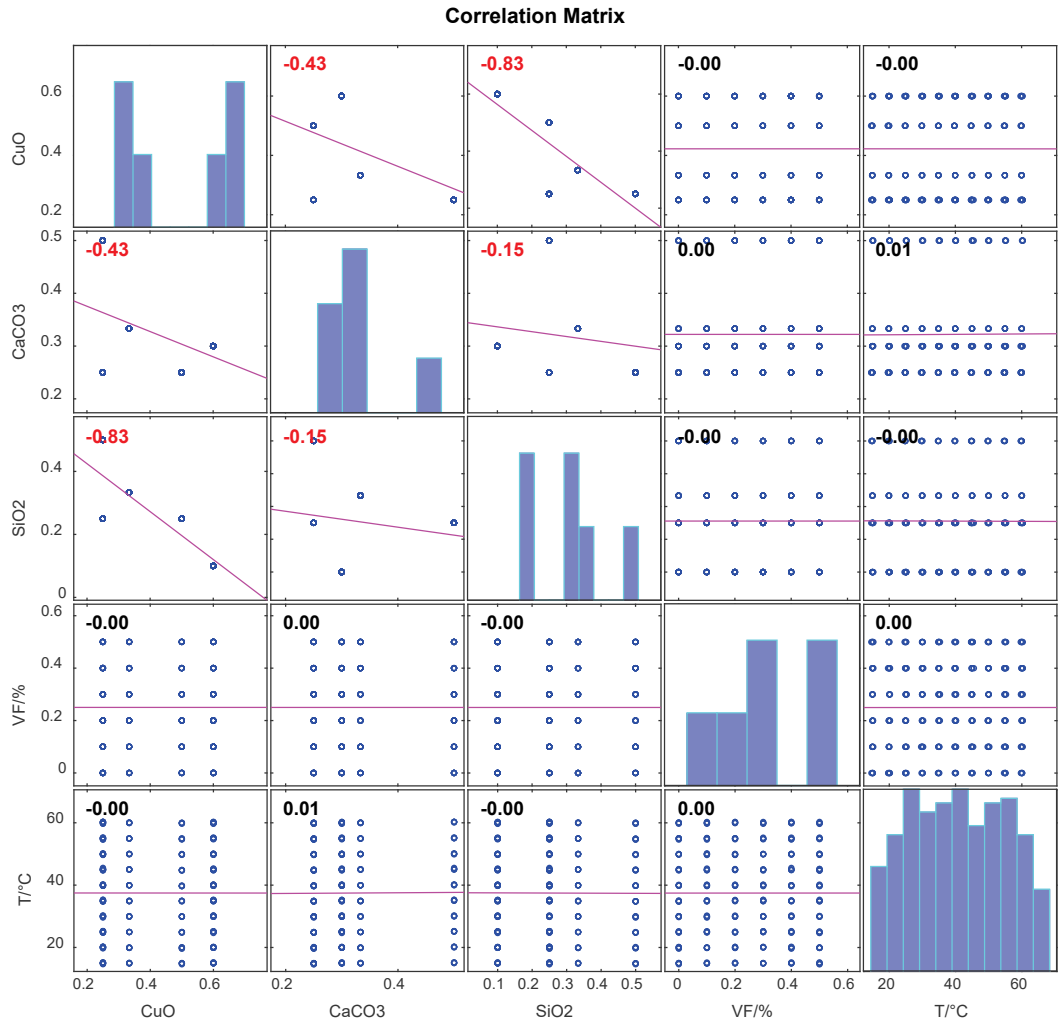

Figure 2. Correlation matrix showing the multicollinearity analysis among the key parameters of the dataset. The matrix displays the Pearson correlation coefficients between input variables (volume ratios of CuO, $CaCO_3$, and SiO_2 nanoparticles, and temperature) and output properties (dynamic viscosity and thermal conductivity).

search space where traditional trial-and-error methods are inefficient and computationally expensive. As a result, integrating optimization algorithms, particularly meta-heuristic methods, has emerged as a promising solution to enhance the predictive performance of SVR models by automating the hyperparameter tuning process.[12,20]

Metaheuristic optimization algorithms are adaptive strategies inspired by natural processes, designed to solve complex optimization problems by efficiently exploring large search spaces.[21] These algorithms offer several advantages over conventional optimization techniques, including their ability to escape local optima and adapt to dynamic problem landscapes. Among these algorithms, the Dragonfly Algorithm (DA) and the FOX-inspired optimization algorithm have demonstrated remarkable efficiency in optimizing machine learning models.[11,22]

The Dragonfly Algorithm (DA) mimics the swarming behavior of dragonflies, which balance exploration (searching broadly through the problem space) and exploitation (refining the search around promising areas).[23] The mathematical framework ofthe DA is based on five critical factors: separation (avoiding overcrowding), alignment (matching velocities), cohesion (sticking together as a group), attraction toward food sources, and distraction from predators. These behavioral patterns allow the algorithm to dynamically adjust its search strategy, making it particularly effective for high-dimensional optimization tasks.[24]

Similarly, the FOX-inspired optimization algorithm is a recent metaheuristic technique introduced by Mohammed et al. in 2022,[25] simulating the adaptive hunting behavior of red foxes in snowy environments. The

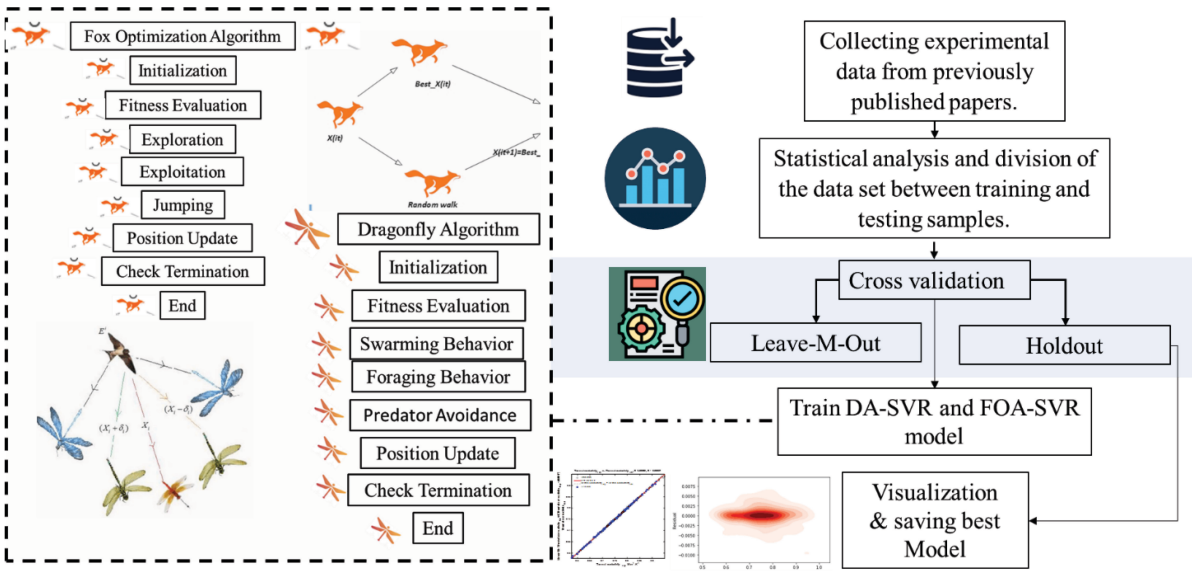

Figure 3. Integration of Dragonfly Algorithm (DA) and FOX-inspired Optimization Algorithm (FOA) with Support Vector Machine for Regression Optimization (SVR). The DA and FOA were applied to generate random hyperparameters for the SVR within predefined ranges. These include the penalty parameter C (0 to 10^6), sigma σ (10^{-3} to 10^2), size of the insensitive zone (ε) (0 to 10^{-2}) and kernel function (Gaussian RBF, linear, and polynomial).[15] This process iterates five times, with the error (e.g., root mean squared error) computed each time the test data is evaluated. The optimal number of search agents and iterations are determined by selecting the model exhibiting the lowest error.

algorithm emulates two phases of hunting: exploration, where the fox uses ultrasound detection to locate prey in uncertain conditions, and exploitation, where it calculates the optimal jump to capture its target[26] (see Figure 3). The algorithm's core strength lies in its balance between global search and local refinement, ensuring it does not get trapped in local optima while efficiently converging toward the global solution.

Hybridizing metaheuristic optimization algorithms with SVR models has become a growing trend in machine learning research, particularly for complex regression tasks.[27] The combination of SVR's capacity to model nonlinear relationships with the adaptive search capabilities of metaheuristic methods results in more robust models capable of handling complex datasets with high-dimensional features. The integration of DA and FOA algorithms in this study highlights the potential of such hybrid approaches in achieving precise and reliable predictions for dynamic viscosity and thermal conductivity in hybrid nanofluids. These advancements contribute to the development of more efficient predictive tools in engineering applications, reducing the need for expensive experimental measurements while ensuring accurate modeling of complex fluid behaviors. Figure 3 present a flowchart of the integration of Dragonfly and FOA Algorithms with SVM for regression optimization.[17]

Cross-Validation Approach

To ensure robust model evaluation and to mitigate the risk of overfitting, two cross-validation techniques were employed in this study: holdout cross-validation and Leave-M-Out cross-validation. Both approaches were used to assess the predictive performance of the SVR models optimized by the Dragonfly Algorithm (DA) and FOX-inspired optimization algorithm (FOA).

Holdout Cross-Validation

In the holdout cross-validation method, the dataset was split into two subsets: 80 % of the data was used for training the model, while the remaining 20 % was reserved for testing. This partitioning was repeated 100 times with random shuffling of the data to ensure that the model's performance was not dependent on a specific split of the data. The holdout method provided an initial assessment of the models' generalization capabilities on unseen data.

Leave-M-Out Cross-Validation

To further validate the robustness of the models, a Leave-M-Out cross-validation technique was applied. In this approach, M = 72 samples were left out from the dataset during each iteration, and the model was trained on the remaining data. The left-out samples were then used to test the model's predictive accuracy. This process was repeated

Table 3. Hyperparameters Results

Method	Model	Penalty parameter $C > 0$	Sigma σ	Size of the insensitive zone (ε)	Kernel function	Quantity of support vectors	Cross validation
DA-SVR	Dynamic viscosity	1.9817×10^5	2.9371	1.2686×10^{-4}	Gaussian RBF	288	Holdout 20 %
	Thermal conductivity	1.2648×10^5	4.6032	6.4220×10^{-6}			
FOA-SVR	Dynamic viscosity	1.8269	1.2971	3.2490×10^{-5}			
	Thermal conductivity	2.8950	1.5342	3.6100×10^{-6}			
DA-SVR	Dynamic viscosity	1.0735×10^3	1.6403	3.3924×10^{-4}			LMO 72
	Thermal conductivity	729.9910	2.6356	3.8428×10^{-6}			
FOA-SVR	Dynamic viscosity	2.8313	1.1793	2.8090×10^{-5}			
	Thermal conductivity	17.2937	1.6752	3.7636×10^{-6}			

100 times with different combinations of left-out samples. This method provides a more comprehensive evaluation by testing the model on various subsets of the data, which helps in identifying any potential weaknesses in the model's generalization ability.

Evaluation Criteria

The accuracy of the model was assessed using various criteria to capture the individual strength of the predictive models, including: mean square error (*MSE*), correlation coefficient (*R*), determination coefficient (R^2), the Theil's U_2, relative standard deviation (*RSD*), mean absolute error (*MAE*), mean relative percentage error (*MRPE*), average absolute relative deviation (*AARD*) and root mean square error (*RMSE*).[28–31] The formulation for each metric is depicted in Equations(1) to (9) as follows:

$$R = \frac{\sum_{i=1}^{n}(y_{i,\text{exp}} - \overline{y}_{i,\text{exp}})\,(y_{i,pri} - \overline{y}_{i,\text{pri}})}{\sqrt{\sum_{i=1}^{n}(y_{i,\text{exp}} - \overline{y}_{i,\text{exp}})^2 \times \sum_{i=1}^{n}(y_{i,pri} - \overline{y}_{i,\text{pri}})^2}} \quad (1)$$

$$MAE = \frac{\sum_{i=1}^{n}\left| y_{i,pri\text{-DA}} - y_{i,\text{exp}} \right|}{n} \quad (2)$$

$$[U_2]_{Thei1} = \left[\frac{\sqrt{\sum_{i=1}^{n}(y_{i,\text{exp}} - y_{i,\text{pri}})^2}}{\sum_{i=1}^{n} {y_{i,\text{exp}}}^2} \right] \quad (3)$$

$$RSD = \frac{\sqrt{\dfrac{\sum_{i=1}^{n}(y_{i,\text{exp}} - y_{i,\text{pri}})^2}{n}}}{\overline{y}_{i,\text{exp}}} \times 100 \quad (4)$$

$$MAE = \frac{\sum_{i=1}^{n}\left| y_{i,\text{exp}} - y_{i,\text{pri}} \right|}{n} \quad (5)$$

$$AARD = 100 \times \frac{\sum_{i=1}^{n}\left(\dfrac{\left| y_{i,\text{exp}} - y_{i,\text{pri}} \right|}{y_{i,\text{exp}}} \right)}{n} \quad (6)$$

$$RMSE = \sqrt{\frac{\sum_{i=1}^{n}(y_{i,\text{exp}} - y_{i,\text{pri}})^2}{n}} \quad (7)$$

$$R^2 = 1 - \frac{\sum_{i=1}^{n}(y_{i,\text{exp}} - y_{i,\text{pri}})^2}{\sum_{i=1}^{n}(y_{i,\text{exp}} - \overline{y}_{i,\text{exp}})^2} \quad (8)$$

where "*n*" is the number of the dataset, "$y_{i,\text{exp}}$" and "$y_{i,\text{pri}}$" are the experimental and predicted values respectively, and "$\overline{y}_{i,\text{exp}}$" is the mean of the experimental values.

RESULTS AND DISCUSSION

This section presents a comprehensive evaluation of the predictive performance of two thermophysical properties: dynamic viscosity and thermal conductivity. These properties were modeled using SVR optimized by Dragonfly Algorithm (DA-SVR) and SVR optimized by FOX-inspired Optimization Algorithm (FOA-SVR). To validate the robustness of the models, two cross-validation techniques were employed: Holdout Cross-Validation (H_CV) and Leave-M-Out Cross-Validation (LMO_CV). The performance of the models was assessed using a set of statistical metrics, including *RMSE*, R^2, *AARD*, *MRPE*, and *MAE*. The hyperparameter results of two optimized models by two algorithms and two cross validation methods are presented in Table 3.

Table 4 summarizes the performance metrics for the DA-SVR and FOA-SVR models in evaluating both dynamic viscosity and thermal conductivity. In overall, the results

Table 4. Statistical metrics and uncertainty of the DA-SVR and FOA-SVR models for the global data set

Method	Dynamic viscosity evaluation Model										
	Data	RMSE	R^2	r	b	slope	AARD	MRPE	MAE	STD	U^2
DA-SVR Holdout_CV	Train	0.0046	0.9997	0.9999	0.0007	0.9991	0.2882	2.6980	0.0024	0.5254	2.50×10^{-5}
	Test	0.0113	0.9984	0.9993	0.0085	0.9907	1.0564	9.2069	0.0084	1.2671	1.44×10^{-4}
	All	0.0065	0.9995	0.9997	0.0023	0.9974	0.4418	9.2069	0.0036	0.7399	4.96×10^{-5}
DA-SVR LMO_CV	Train	0,0058	0,9996	0,9998	–0,0003	1,0010	0,3989	2,9194	0,0033	0,6743	$4{,}11 \times 10^{-5}$
	Test	0,0047	0,9997	0,9998	0,0011	0,9990	0,3358	2,8646	0,0026	0,5520	$2{,}75 \times 10^{-5}$
	All	0,0059	0,9996	0,9998	–0,0004	1,0010	0,4042	3,8344	0,0034	0,6713	$4{,}09 \times 10^{-5}$
FOA-SVR Holdout_CV	Train	0,0051	0,9997	0,9998	0,0004	0,9999	0,3247	2,6191	0,0027	0,5790	3.03×10^{-5}
	Test	0,0077	0,9992	0,9996	0,0043	0,9965	0,7226	2,8909	0,0060	0,8733	6.88×10^{-5}
	All	0,0057	0,9996	0,9998	0,0012	0,9992	0,4043	2,8909	0,0034	0,6491	3.82×10^{-5}
FOA-SVR LMO_CV	Train	0,0055	0,9996	0,9998	–0,0005	1,0006	0,3666	3,5994	0,0030	0,6410	$3{,}71 \times 10^{-5}$
	Test	0,0044	0,9997	0,9999	–0,0025	1,0020	0,3239	3,0708	0,0026	0,4758	$2{,}05 \times 10^{-5}$
	All	0,0053	0,9996	0,9998	–0,0008	1,0008	0,3581	3,5994	0,0029	0,6075	$3{,}35 \times 10^{-5}$
Method	Thermal conductivity evaluation Model										
	Data	RMSE	R^2	r	b	slope	AARD	MRPE	MAE	STD	U^2
DA-SVR Holdout_CV	Train	0,0020	0,9994	0,9997	0,0015	0,9978	0,1524	1,0197	0,0012	0,2647	$6{,}89 \times 10^{-6}$
	Test	0,0025	0,9991	0,9996	0,0025	0,9968	0,2700	1,1255	0,0020	0,3432	$1{,}15 \times 10^{-5}$
	All	0,0021	0,9994	0,9997	0,0017	0,9976	0,1759	1,1255	0,0013	0,2813	$7{,}79 \times 10^{-6}$
DA-SVR LMO_CV	Train	0,0019	0,9995	0,9997	0,0009	0,9988	0,1603	0,9802	0,0012	0,2614	$6{,}72 \times 10^{-6}$
	Test	0,0020	0,9993	0,9997	0,0005	0,9992	0,1672	0,8912	0,0013	0,2641	$6{,}80 \times 10^{-6}$
	All	0,0020	0,9995	0,9997	0,0008	0,9988	0,1617	0,9802	0,0012	0,2616	$6{,}74 \times 10^{-6}$
FOA-SVR Holdout_CV	Train	0.0018	0.9996	0.9998	0.0010	0.9986	0.1347	0.8730	0.0010	0.2354	$5{,}45 \times 10^{-6}$
	Test	0.0024	0.9991	0.9994	–0.0028	1.0038	0.2469	0.9356	0.0019	0.3161	$9{,}77 \times 10^{-6}$
	All	0.0019	0.9995	0.9997	0.0005	0.9993	0.1571	0.9356	0.0012	0.2533	$6{,}32 \times 10^{-6}$
FOA-SVR LMO_CV	Train	0,0019	0,9995	0,9997	0,0010	0,9987	0,1544	1,0643	0,0012	0,2607	$6{,}68 \times 10^{-6}$
	Test	0,0020	0,9993	0,9997	0,0006	0,9994	0,1673	0,8570	0,0012	0,2645	$6{,}83 \times 10^{-6}$
	All	0,0019	0,9995	0,9997	0,0012	0,9983	0,1553	1,0643	0,0012	0,2590	$6{,}60 \times 10^{-6}$

indicate excellent performance on the training data and good generalizability to unseen test data for both properties.

Dynamic Viscosity Model Result

For the dynamic viscosity predictions, the DA-SVR model demonstrated strong performance under both cross-validation methods as indicated in Tables 3 and 4.

With the H_CV method, the model achieved an RMSE of 0.0113 and an R^2 of 0.9984, indicating high accuracy in predicting test data. The hyperparameters for this configuration included a penalty parameter (C) of 1.9817×10^5, a sigma (σ) of 2.9371, and an insensitive zone (ε) of 1.2686×10^{-4}, reflecting a relatively rigid model structure aimed at minimizing error. Using LMO_CV, the DA-SVR model's performance improved significantly, with an RMSE of 0.0047 and an R^2 of 0.9997, while the hyperparameters $C = 1.0735 \times 10^3$, $\sigma = 1.6403$, $\varepsilon = 3.3924 \times 10^{-4}$ indicate a more flexible configuration than that used in H_CV.

In contrast, the FOA-SVR model consistently outperformed DA-SVR in terms of generalization to test data. Under H_CV, FOA-SVR achieved an *RMSE* of 0.0077 and an R^2 of 0.9992, showing reduced prediction error and improved correlation compared to DA-SVR. The hyperparameters $C = 1.8269$, $\sigma = 1.2971$, $\varepsilon = 3.2490 \times 10^{-5}$ illustrate its focus on achieving smoother decision boundaries. With LMO_CV, FOA-SVR delivered even stronger results, achieving an *RMSE* of 0.0044 and an R^2 of 0.9997. The hyperparameters, $C = 2.8313$, $\sigma = 1.1793$, and $\varepsilon = 2.8090 \times 10^{-5}$, emphasize the model's ability to generalize effectively while maintaining high precision.

Thermal Conductivity Model Result

For thermal conductivity predictions, the DA-SVR model

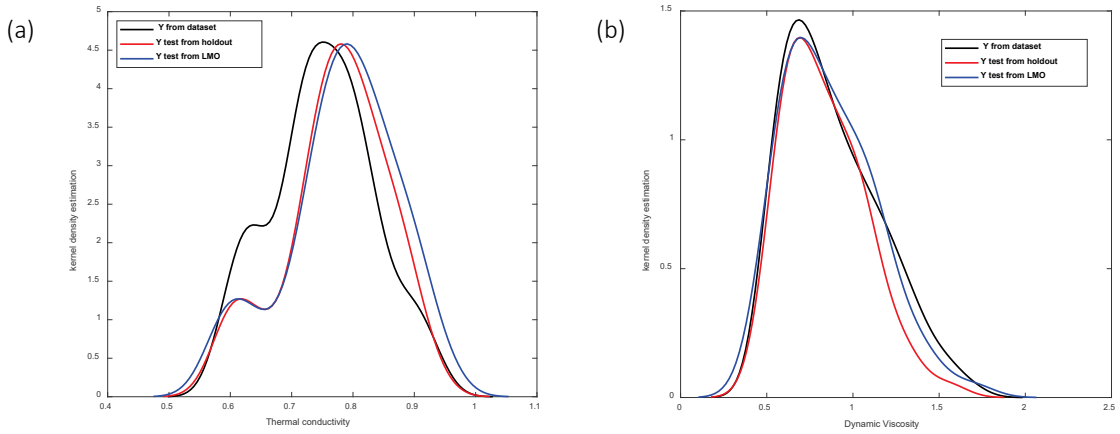

Figure 4. Kernel Density Estimate (KDE) plot illustrating the distribution of thermal conductivity data (Figure 4(a)) and dynamic viscosity (Figure 4(b)) for the original dataset (in black) compared to the data test values obtained from two cross-validation methods: Holdout (in red) and Leave-M-Out (LMO) (in blue).

performed well but showed slightly higher error metrics compared to the FOA-SVR model. Under H_CV, DA-SVR achieved an *RMSE* of 0.0025 and an R^2 of 0.9991. While these values confirm strong predictive accuracy. The optimal hyperparameters got for this configuration C = 1.2648×10^5, σ = 4.6032, $\varepsilon = 6.4220 \times 10^{-6}$ indicate a rigid model configuration. The LMO_CV method improved the model's performance, yielding an *RMSE* of 0.0020 and an R^2 of 0.9993. The hyperparameters C = 729.9910, σ = 2.6356, $\varepsilon = 3.8428 \times 10^{-6}$ highlight a more balanced trade-off between error minimization and flexibility.

The FOA-SVR model showed same errors results but high signification of hyperparameters. Using H_CV, the model achieved an *RMSE* of 0.0024 and an R^2 of 0.9991. Hyperparameters C = 2.8950, σ = 1.5342, $\varepsilon = 3.6100 \times 10^{-6}$ demonstrate the model's adaptability and focus on smoother decision boundaries. Under LMO_CV, the FOA-SVR model delivered excellent results, with an RMSE of 0.0020 and an R^2 of 0.9993. The hyperparameters C = 17.2937, σ = 1.6752, $\varepsilon = 3.7636 \times 10^{-6}$ further emphasize the model's ability to generalize effectively while achieving precise predictions.

Leave-M-Out Cross-Validation (LMO_CV) and Holdout Cross-Validation (H_CV) Comparative Results

Figures 4.a and 4.b display Kernel Density Estimates (KDE) plots that compare the distribution of thermal conductivity and dynamic viscosity values between the original dataset and the test data selected using two cross-validation methods: Holdout and Leave-M-Out (LMO). The KDE plots reveal that the distributions of the test data obtained from both Holdout and LMO closely mirror the distribution of the original dataset. While minor discrepancies in the means and spread of the distributions exist, these differences are insignificant. Notably, the LMO-selected test data appears to more accurately reflect the original dataset, especially for dynamic viscosity, suggesting better generalization. These findings explain why LMO_CV performed slightly better than H_CV. Given that LMO_CV and FOA-SVR achieved the best results, our subsequent research has focused on these methods.

Comparative Between FOA-SVR and DA-SVR Models

The comparison between the DA-SVR and FOA-SVR models reveals significant differences in their approaches to achieving predictive accuracy and generalization. Both models demonstrated excellent results, with R^2 values consistently exceeding 0.999, but the FOA-SVR model consistently delivered lower *RMSE* values, indicating better error minimization. A critical factor contributing to this difference is the selection of hyperparameters. The FOA-SVR model selected significantly lower penalty parameters (C) and sigma (σ) values, which resulted in smoother decision boundaries and a reduced risk of overfitting. This adaptability enabled FOA-SVR to generalize better across unseen data, particularly in the LMO_CV method. Another distinguishing feature is the performance of the two models under different cross-validation techniques. While DA-SVR showed noticeable improvements when switching from H_CV to LMO_CV, FOA-SVR demonstrated robust performance across both methods. This consistency highlights the FOX-inspired optimization algorithm's ability to balance exploration and exploitation during hyper-parameter tuning, leading to a more reliable model.

In overall, the FOA-SVR model's superior generalization capabilities and its ability to maintain low bias and error metrics across diverse datasets make it the preferred choice for predicting dynamic viscosity and thermal conductivity. The FOX-inspired optimization

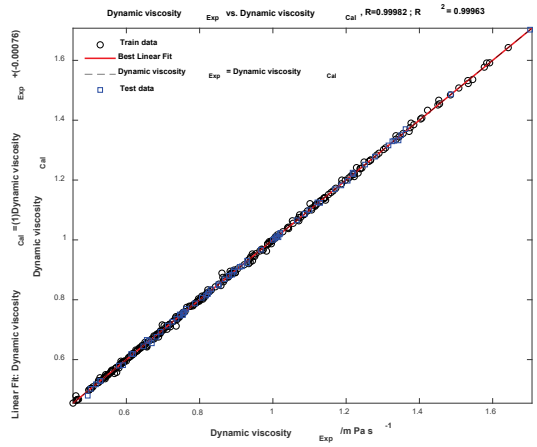

Figure 5. Regression plot showing the predicted versus actual values of dynamic viscosity for the test dataset and the entire dataset using the FOA-SVR-LMO_CV model. The diagonal line represents the ideal fit where predicted values perfectly match the actual values. Data points closer to this line indicate better predictive performance. The distribution and spread of points provide insights into the model's accuracy and generalization capability across the dataset.

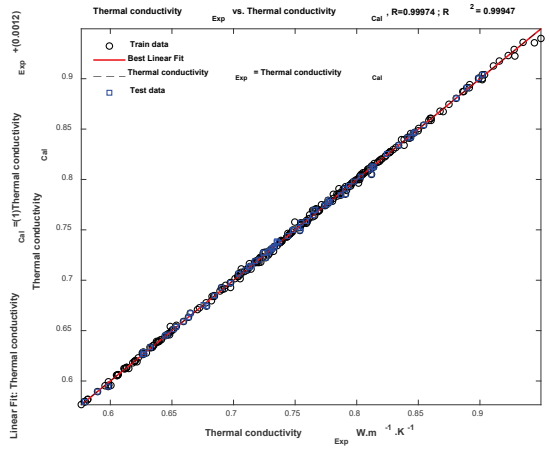

Figure 6. Illustrates the regression plot comparing predicted and actual thermal conductivity values. The FOA-SVR-LMO_CV model's performance is evaluated on both the test dataset and the entire dataset. The diagonal line represents the ideal scenario where predictions perfectly match actual values. Data points closer to this line signify higher predictive accuracy. The overall distribution and dispersion of these points offer valuable insights into the model's accuracy and its ability to generalize well across the entire dataset.

algorithm offers a refined strategy for hyperparameter tuning, making it a valuable tool for complex regression tasks requiring high accuracy and reliability.

The regression plots in Figures 5 and 6 offer a visual representation of the relationship between predicted and

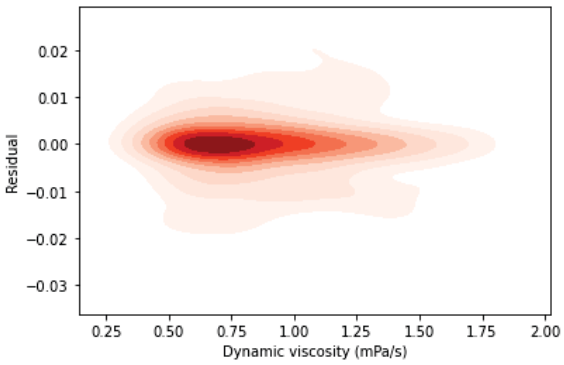

Figure 7. Kernel Density Estimate (KDE) plot of the residuals for dynamic viscosity predictions (mPa·s^{-1}) using the FOA-SVR-LMO_CV model. The plot illustrates the distribution of prediction errors, with the density curve highlighting that most residuals are centered around zero. This indicates that the FOA-SVR model provides highly accurate predictions with minimal deviation between observed and predicted values.

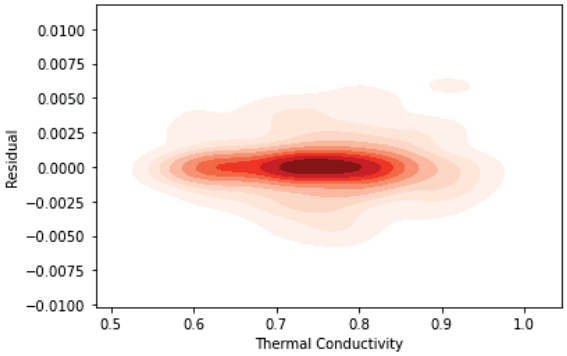

Figure 8. Kernel Density Estimate (KDE) plot of the residual values between the predicted and actual thermal conductivity using the FOA-SVR-LMO_CV model. The density curve, shown in dark color, highlights the distribution of residuals, with the majority clustering around zero. This indicates that the FOA-SVR model achieves high accuracy, with minimal deviation between the predicted and actual values.

actual values for both dynamic viscosity and thermal conductivity. The plot for dynamic viscosity illustrates a strong positive correlation, with the majority of data points closely following a diagonal line with a slope close to 1. This visually confirms the high R^2 values (> 0.99) observed, indicating a strong linear relationship between predicted and actual viscosity values.

Furthermore, Figures 7 and 8 present the Kernel Density Estimation (KDE) plots for the residuals, representing the differences between the experimental and predicted values obtained by the FOA-SVR model for dynamic viscosity and thermal conductivity, respectively.

The KDE plots indicate that the residuals are densely concentrated around zero, suggesting that the FOA-SVR model provides accurate predictions with minimal error; this reduced dispersion of residuals reflects the model's ability to generalize well across the dataset, minimizing overfitting and ensuring reliable predictions for both dynamic viscosity and thermal conductivity.

Comparison with previously published models

To assess the predictive performance of the developed models, we compared their accuracy with previously reported models from the literature, using the statistical metrics presented in Table 5. While the training and test datasets used in this study differ from those in Refs. [31] and [32], the results indicate that the accuracy of our FOA-SVR and DA-SVR models is on a comparable level. Given the differences in datasets, a direct comparison may not be fully conclusive; nevertheless, the low error values and high correlation coefficients achieved by our models demonstrate their potential to effectively predict both thermal conductivity and dynamic viscosity in hybrid ternary nanofluids. The consistent accuracy across the training, testing, and overall datasets underscores the robustness of our approach and aligns well with previously published results. Future studies could further validate these findings by applying our models to the same datasets used in Refs. [31] and [32] to establish a more direct performance comparison.

CONCLUSION

This study developed and evaluated four machine learning models: DA-SVR with H_CV, DA-SVR with LMO_CV, FOA-SVR with H_CV, and FOA-SVR with LMO_CV. All models demonstrated exceptional predictive capabilities, achieving R^2 values exceeding 0.999 across all datasets, underscoring their accuracy and reliability; moreover, a detailed comparison revealed the superior performance of the FOA-SVR models, which consistently outperformed DA-SVR models in terms of error minimization and generalization. The differences in performance can be attributed to the hyperparameter selection and the used optimization techniques. The FOX-inspired optimization algorithm employed in FOA-SVR allowed for the selection of lower penalty parameters (C) and sigma (σ) values, leading to smoother decision boundaries and better generalization to unseen data. In contrast, DA-SVR models, while robust, exhibited a relatively rigid structure that limited their flexibility in certain scenarios; furthermore, the FOA-SVR models maintained consistent performance across both Holdout and LMO cross-validation methods, emphasizing their reliability and adaptability to various data splits. The role of cross-validation methods was also crucial in evaluating the models. The LMO_CV method proved to be more robust, consistently producing lower RMSE values and higher R^2 values compared to H_CV; this highlights the importance of using comprehensive validation techniques to ensure the reliability and generalizability of machine learning models.

The findings of this study have significant implications for the accurate modeling and prediction of thermophysical properties in advanced nanofluids. The FOA-SVR models' superior performance makes them valuable tools for industrial applications requiring precise and reliable predictions, such as in energy systems, thermal management, and advanced manufacturing. Future research could explore the integration of hybrid optimization techniques or the extension of these models to predict additional thermophysical properties, further enhancing their utility and applicability. Future work may explore the application of hybrid or multi-objective optimization techniques to further enhance the performance of these models in predicting other thermophysical properties of nanofluids.

Table 5. Accuracy of the developed DA-SVR model for THNFs compared with previously published models

Ref.	Nanoparticles/Base fluid	Models	Data points	Inputs	Output	Statistical metrics		
						R/R^2	U^2	MSE/RMSE
[29]	MWCNT-TiO2-ZnO / DW	ANN	102	nanofluid type, φ and T	λ_{thnf}	0.9951	/	-2.0402×10^{-5} /
[30]	rGO-Fe_3O_4-TiO_2 / EG	BRT	1264	T and wt %	λ_{thnf}	0.9989 0.9978	0.0689	/ 0.0006
				T, γ, and wt %	μ	0.9979 0.9959	0.121	/ 0.0004
This study	CuO-$CaCO_3$-SiO_2 / DW	FOA-SVR	360	nanofluid type, φ and T	λ_{thnf}	0.9997 0.9995	3.91×10^{-5}	/ 0,0019
					μ	0,9998 0,9996	6.32×10^{-6}	/ 0,0053

ABBREVIATIONS

AARD	Average Absolute Relative Deviation
BRT	Boosted Regression Tree
R	Correlation coefficients
R^2	Determination coefficients
DW	Distilled water
DA	Dragonfly Algorithm
μ	Dynamic viscosity/ mPa s^{-1}
EG	Ethylene Glycol
FOA	FOX-inspired Optimization Algorithm
H_CV	Holdout Cross-Validation
IQR	InterQuartile Range
KDE	Kernel Density Estimation
LMO	Leave-M-Out
LMO_CV	Leave-M-Out Cross-Validation
MAE	Mean Absolute Error
MRPE	Mean Relative Percentage Error
MSE	Mean Squared Error
MWCNT	Multi-Walled Carbon Nanotubes
RSD	Relative Standard Deviation
RMSE	Root Mean Square Error
SDS	Sodium dodecyl sulfate
VF%	Solid volume concentration
STD	STandard Deviation
SVM	Support Vector Machine
SVR	Support Vector Regression
DA-SVR	Support Vector Regression model optimized by the Dragonfly Algorithm
FOA-SVR	Support Vector Regression model optimized by the FOX-inspired Optimization Algorithm
T	Temperature
λ_{thnf}	Thermal conductivity of trihybrid nanofluids / W m^{-1} K^{-1}
THNFs	TriHybrid NanoFluids
φ	Volume fraction of nanoparticles

Acknowledgment. The authors extend their heartfelt gratitude to Abderrahmene Euldji for his assistance with the English language. They also acknowledge the support provided by the Direction Générale de la Recherche Scientifique et Développement Technologique (DGRSDT), Algeria.

Supplementary Information. The dataset is provided in the supplementary material, and the code can be accessed via the following link: https://github.com/med-hentabli/FOA-SVM-with-LMO-CV.git and attached to the electronic version of the article at: https://doi.org/10.5562/cca4137.

PDF files with attached documents are best viewed with Adobe Acrobat Reader which is free and can be downloaded from Adobe's web site.

REFERENCES

[1] H. Adun, D. Kavaz, M. Dagbasi, *J. Clean. Prod.* **2021**, *328*, 129525. https://doi.org/10.1016/j.jclepro.2021.129525

[2] N. Sezer, M. A. Atieh, M. Koç, *Powder Technol.* **2019**, *344*, 404–431. https://doi.org/10.1016/j.powtec.2018.12.016

[3] J. P. Vallejo, J. I. Prado, L. Lugo, *Appl. Therm. Eng.* **2022**, *203*, 117926. https://doi.org/10.1016/j.applthermaleng.2021.117926

[4] M. Hemmat Esfe, S. Esfandeh, E. Hosseinizadeh, *Int. Commun. Heat Mass Transf.* **2020**, *118*, 104810. https://doi.org/10.1016/j.icheatmasstransfer.2020.104810

[5] C. J. Ho, C. Y. Chang, W.-M. Yan, *Int. Commun. Heat Mass Transf.* **2017**, *83*, 23–29. https://doi.org/10.1016/j.icheatmasstransfer.2017.03.002

[6] E. Shahsavani, M. Afrand, R. Kalbasi, *Appl. Therm. Eng.* **2018**, *129*, 1573–1581. https://doi.org/10.1016/j.applthermaleng.2017.10.140

[7] M. Kouider Amar, S. Rahal, M. Laidi, R. Rebhi, M. Hentabli, S. Hanini, M. Hamadache, *J. Pharm. Innov.* **2022**, *17*, 1434–1450. https://doi.org/10.1007/s12247-022-09642-0

[8] V. V. Wanatasanappan, M. Z. Abdullah, P. Gunnasegaran, *J. Mol. Liq.* **2020**, *313*, 113458. https://doi.org/10.1016/j.molliq.2020.113458

[9] K. A. Hamid, W. H. Azmi, M. F. Nabil, R. Mamat, K. V. Sharma, *Int. J. Heat Mass Transf.* **2018**, *116*, 1143–1152. https://doi.org/10.1016/j.ijheatmasstransfer.2017.09.087

[10] M. Hemmat Esfe, P. M. Behbahani, A. A. A. Arani, M. R. Sarlak, *J. Therm. Anal. Calorim.* **2017**, *128*, 249–258. https://doi.org/10.1007/s10973-016-5893-9

[11] M. Hentabli, M. Kouider Amar, A.-E. Belhadj, *Int. J. Environ. Anal. Chem.* **2024**, 1–26. https://doi.org/10.1080/03067319.2024.2382374

[12] A. Chabane, F. Bouchal, M. Hentabli, N. Ayachi, H. E. Slama, F. Rezgui, L. Hammoumraoui, *Can. J. Chem. Eng.* **2023**, *101*, 4446–4459. https://doi.org/10.1002/cjce.24811

[13] F. Omari, L. Khaouane, M. Laidi, A. Ibrir, M. Roubehie Fissa, M. Hentabli, S. Hanini, *Comput. Methods Biomech. Biomed. Engin.* **2023**, 1–10.

[14] M. Hemmat Esfe, A. Tatar, M. R. H. Ahangar, H. Rostamian, *Phys. E Low-dimensional Syst. Nanostructures* **2018**, *96*, 85–93. https://doi.org/10.1016/j.physe.2017.08.019

[15] M. Mousavi, A. Pouranfard, P. Darvishi, *Colloids Surfaces A Physicochem. Eng. Asp.* **2024**, *686*, 133367. https://doi.org/10.1016/j.colsurfa.2024.133367
[16] S. Tripathi, V. V Srinivas, R. S. Nanjundiah, *J. Hydrol.* **2006**, *330*, 621–640. https://doi.org/10.1016/j.jhydrol.2006.04.030
[17] H. Moussa, F. Dahmoune, M. Hentabli, H. Remini, L. Mouni, *Chemom. Intell. Lab. Syst.* **2022**, *222*, 104493. https://doi.org/10.1016/j.chemolab.2022.104493
[18] H. Benimam, C. S. Moussa, M. Hentabli, S. Hanini, M. Laidi, *J. Chem. Eng. Data* **2020**, *65*, 3161–3172. https://doi.org/10.1021/acs.jced.0c00168
[19] R. Moumen, M. Laidi, S. Hanini, M. Hentabli, A. Ibrir, *Kem. u Ind.* **2023**, *72*, 169–178. https://doi.org/10.15255/KUI.2022.048
[20] A. Chabane, F. Bouchal, M. Hentabli, F. Rezgui, H. E. Slama, *Kem. u Ind.* **2022**, *71*, 9–19. https://doi.org/10.15255/KUI.2021.008
[21] M. Hentabli, A.-E. Belhadj, H. Benimam, F. Dahmoune, S. Keskes, *Powder Technol.* **2021**, *383*, 220–232. https://doi.org/10.1016/j.powtec.2021.01.038
[22] M. Hentabli, A. E. Belhadj, F. Dahmoune, *Kem. u Ind.* **2021**, *70*, 501–508. https://doi.org/10.15255/KUI.2020.073
[23] S. Mirjalili, *Neural Comput. Appl.* **2016**, *27*, 1053–1073. https://doi.org/10.1007/s00521-015-1920-1
[24] L. Hadjout-Krimat, A. Belbahi, F. Dahmoune, M. Hentabli, A. Boudria, S. Achat, H. Remini, S. Oukhmanou-Bensidhoum, G. Spigno, K. Madani, *J. Food Process Eng.* **2023**, *46*, e14232. https://doi.org/10.1111/jfpe.14232
[25] H. Mohammed, T. Rashid, *Appl. Intell.* **2023**, *53*, 1030–1050. https://doi.org/10.1007/s10489-022-03533-0
[26] Z. Zhang, X. Wang, L. Cao, *Biomimetics* **2024**, *9*, 524. https://doi.org/10.3390/biomimetics9090524
[27] M. F. Fadhillah, S. Lee, C.-W. Lee, Y.-C. Park, *Remote Sens.* **2021**, *13*, 1196. https://doi.org/10.3390/rs13061196
[28] R. Rostamzadeh-Renani, M. Baghoolizadeh, S. Mohammad Sajadi, M. Pirmoradian, M. Rostamzadeh-Renani, S. Baghaei, S. Salahshour, *Alexandria Eng. J.* **2023**, *84*, 184–203. https://doi.org/10.1016/j.aej.2023.10.059
[29] M. Hemmat Esfe, S. Saedodin, *Exp. Therm. Fluid Sci.* **2014**, *55*, 1–5. https://doi.org/10.1016/j.expthermflusci.2014.02.011
[30] M. Umar, Z. Sabir, M. A. Z. Raja, Y. G. Sánchez, *Results Phys.* **2020**, *19*, 103585. https://doi.org/10.1016/j.rinp.2020.103585
[31] Z. Said, N. K. Cakmak, P. Sharma, L. S. Sundar, A. Inayat, O. Keklikcioglu, C. Li, *Powder Technol.* **2022**, *400*, 117190. https://doi.org/10.1016/j.powtec.2022.117190
[32] X. Yang, A. Boroomandpour, S. Wen, D. Toghraie, F. Soltani, *Powder Technol.* **2021**, *388*, 418–424. https://doi.org/10.1016/j.powtec.2021.04.093